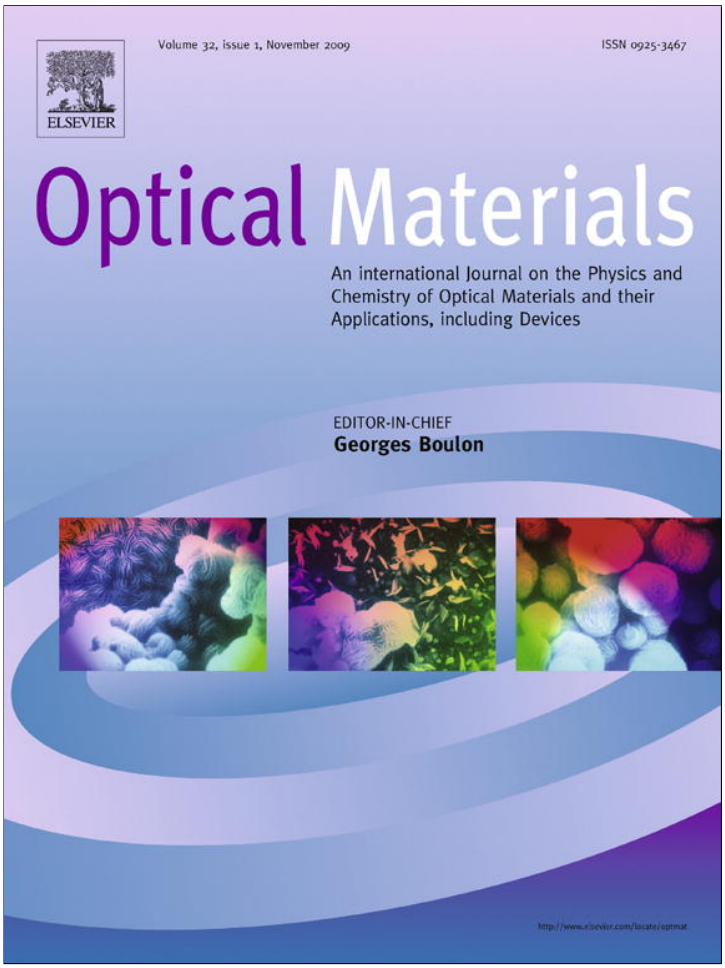

Optical Materials 32 (2009) 30–34

Contents lists available at ScienceDirect

Optical Materials

journal homepage: www.elsevier.com/locate/optmat

Influence of erbium doping on phase transition and optical properties of strontium barium niobate

Isabella-Ioana Oprea [1], Uwe Voelker, Alexander Niemer, Rainer Pankrath, Sergey Podlozhenov [2], Klaus Betzler *

Fachbereich Physik, Universität Osnabrück, D-49069 Osnabrück, Germany

ARTICLE INFO

Article history:
Received 24 April 2009
Received in revised form 26 May 2009
Accepted 27 May 2009
Available online 26 June 2009

PACS:
78.55.Hx
78.40.Ha
77.84.Dy
71.55.Ht

Keywords:
Strontium barium niobate
Erbium
Luminescence
Phase transition

ABSTRACT

The optical properties of erbium impurities in strontium barium niobate are investigated measuring optical absorption and emission in the visible and near infrared spectral region. For the main fluorescence band at 1.55 μm, an anomalous dependence of the fluorescence decay time on dopant concentration is found which, however, can be consistently explained by reabsorption effects. A Judd–Ofelt analysis of the absorption spectra together with an appropriate analysis of the reabsorption yields a radiative quantum efficiency of approximately 60%. In addition, erbium dopants are shown to efficiently influence the phase transition temperature of strontium barium niobate.

1. Introduction

Triply ionized erbium atoms, Er^{3+}, are widely used as infrared fluorescent agents in different glasses for broadband optical amplifiers in data transmission lines (*E*rbium *D*oped *F*iber *A*mplifiers, EDFAs). Crystalline host materials could extend these applications, e.g., to integrated amplifiers and to self-frequency converting lasers. One of the most promising host material for such applications is strontium barium niobate, $Sr_xBa_{1-x}Nb_2O_6$ – henceforth denoted as SBN. Due to its interesting dielectric, photorefractive, electro-optic, and nonlinear optic properties, the solid solution SBN has gained considerable interest for potential applications. These include pyroelectric detection [1], surface acoustic wave devices [2], electro-optic modulation [3], holographic data storage [4], phase conjugation [5], and the generation of photorefractive solitons [6]. High nonlinear optical coefficients make it suitable for quasi-phase-matched [7] or random optical frequency doubling [8–10].

SBN crystallizes in a tetragonal tungsten bronze structure over a wide solid solution range, the existence region of this tetragonal phase could be recently determined [11] to be $0.26 \leqslant x \leqslant 0.87$ (experimentally as single crystals realized $0.32 \leqslant x \leqslant 0.82$). Throughout this tetragonal phase, SBN is ferroelectric at low temperatures (point group 4 mm, space group P 4 b m) and paraelectric at high temperatures (point group 4/m mm, space group P 4/m b m). The phase transition of SBN is of relaxor type (see e.g., [12]), the transition temperatures depend on the composition and vary from 290 K ($x = 0.82$) to 500 K ($x = 0.32$) [13]. The exact type of the phase transition is still controversely discussed (see [14–16], and references cited therein).

Dopants have been shown to modify the properties of SBN distinctly. Thus, e.g., the phase transition temperature can be greatly varied by doping with cerium and chromium [17] or with europium [18]. Luminescent dopants can be used to tailor the fluorescence properties of SBN for various novel applications. Neodymium doping allows for coherent light generation [19,20] and for self frequency conversion [21,22]. Other trivalent lanthanide ions have been characterized and tested for applications, too (see, e.g., Refs. [23–30]).

In this work, we present comprehensive results on Er^{3+} in SBN concerning distribution coefficients, influence on the phase transition, optical absorption and emission.

* Corresponding author.
E-mail address: klaus.betzler@uni-osnabrueck.de (K. Betzler).
[1] Present address: TU Berlin, FG EvUR, D-10623 Berlin, Germany.
[2] Present address: Rubicon Technology, Franklin Park, IL 60131, USA.

0925-3467/$ - see front matter © 2009 Elsevier B.V. All rights reserved.
doi:10.1016/j.optmat.2009.05.015

2. Results and discussion

The crystals for our investigations were grown from the congruently melting composition of SBN ($Sr_xBa_{1-x}Nb_2O_6$ with $x = 0.61$) using the Czochralski technique. Details of the growth process are described in Ref. [11]. Er_2O_3 was added to the melt in a series ranging from 0 to 2 mol%.

2.1. Distribution coefficient

The erbium content in the crystals was determined using accurate X-ray fluorescence measurements, for details of the measurement and the evaluation procedure see Ref. [11]. The distribution coefficient d – the ratio between crystal and melt concentrations – was found to be approximately constant in our doping range

$$d = c_{Er}^{crystal}/c_{Er}^{melt} = 0.54 \pm 0.02. \quad (1)$$

Compositions given throughout this article will refer to the crystal concentration, i.e., the molar percentage of Er per Nb or – which is accordingly equal – the molar percentage of Er_2O_3 per $Sr_xBa_{1-x}Nb_2O_6$.

2.2. Phase transition temperature as a function of Er doping

SBN undergoes a structural phase transition from a ferroelectric low-temperature to a paraelectric high-temperature phase at a temperature $T_i = 350$ K (for $x = 0.61$). This transition temperature depends distinctly on composition and doping concentration.

Usually this transition temperature is yielded from direct pyroelectric measurements of the polarization decay when heating previously poled samples [13]. To get this transition temperature, however, both, for heating *and* for cooling, we measured the temperature dependence of the optical second harmonic intensity, $I_{SHG}(T)$, on unpoled samples. As fundamental light source a pulsed Nd:YAG-laser was used (repetition rate 20 Hz, pulse width 5 ns, pulse energy 50 mJ). The samples' heating and cooling rate during the measurements was approximately 40 K/h.

The second harmonic intensity is proportional to the square of the effective tensor element of the second order nonlinear susceptibility, which in turn is proportional to the ferroelectric polarization,

$$I_{SHG}(T) \propto d_{eff}^2(T) \propto P^2(T). \quad (2)$$

Thus from the second harmonic measurements the temperature dependence of the ferroelectric polarization $P(T)$ for heating and for cooling can be derived. The inflection point T_i of this temperature dependence usually is regarded as the transition temperature or – better – as the center of the transition region (Curie region) in a relaxor ferroelectric [17].

The results of these measurements are summarized in Fig. 1. The thus defined transition temperatures T_i depend linearly on the erbium concentration c_{Er} both for heating (up) and cooling (dn)

$$T_{i,\,up} = -26.6c_{Er} + 351.0, \quad (3)$$

$$T_{i,\,dn} = -32.3c_{Er} + 347.8 \ (c_{Er} \text{ in mol\%}, \ T_i \text{ in K}). \quad (4)$$

The phase transition is strongly shifted to lower temperatures with increasing erbium content. The difference between the two values $T_{i,\,up}$ and $T_{i,\,dn}$, i.e., the phase transition's hysteresis, increases, indicating an increase in the *relaxor* behavior. Erbium, thus, besides defining the optical properties, turns out to be an effective tool for modifying the phase transition properties of SBN.

2.3. Absorption spectra

The polarized absorptions spectra were measured in the visible and near infrared spectral regions using a Bruins Instruments Omega 10 spectrometer. The results for the three relevant polarizations – $\boldsymbol{\alpha}$,$\boldsymbol{\pi}$, and $\boldsymbol{\sigma}$ –, are depicted in Fig. 2. All transitions are starting from the ground state level $^4I_{15/2}$. The absorption bands are labeled each with the excited state level involved in the respective transition. The assignments are made according to the data for the free-ion energy level scheme of Er^{3+} given by Dieke [31].

The measurements were performed both, at room temperature (300 K) and at a temperature of 10 K. At both temperatures the spectra show a distinct broadening of all absorption lines which is only slightly more expressed at the higher temperature. That even the low temperature spectra show broad lines, can be explained by statistical variations in the environment of the dopant ions. Due to EXAFS measurements [28] erbium ions occupy niobium sites. For these sites, the first nearest neighbor shell consists of six oxygens. Due to the unfilled tungsten bronze structure of SBN, the second nearest neighbor shell, however, is characterized by a statistical distribution of barium-occupied, strontium-occupied, and empty sites. This results in a large number of different environments and, accordingly, in a respective

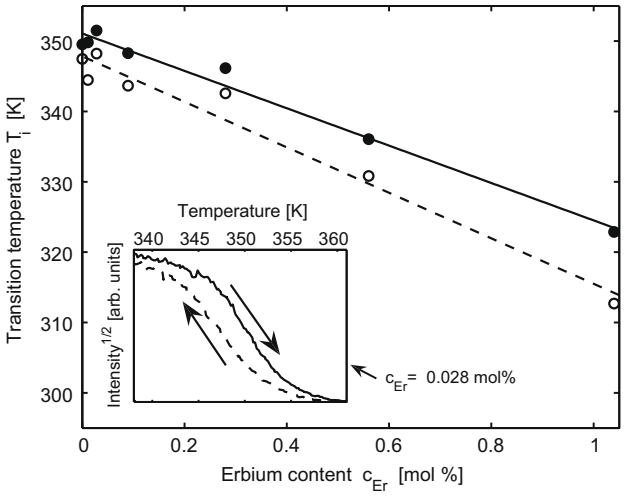

Fig. 1. Transition temperature T_i (i.e., inflection point) of the ferroelectric polarization as a function of the erbium content in SBN. Full circles: heating, open circles: cooling. The lines are linear fits to the experimental data. In the inset a typical measurement of the heating and cooling behavior is shown.

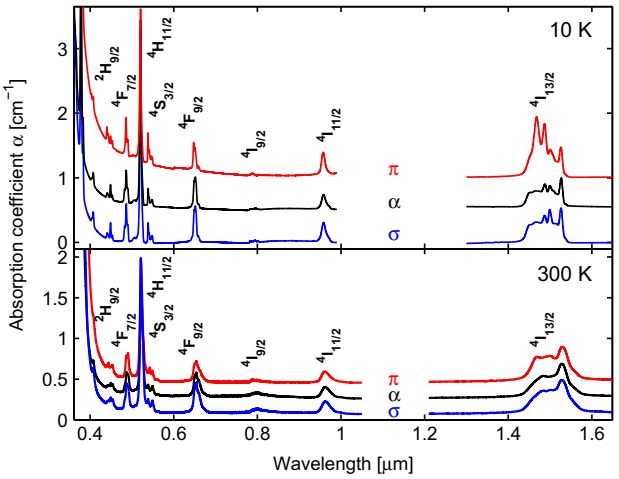

Fig. 2. Absorption lines of erbium ions in SBN in the visible and near infrared spectral regions for the three polarizations $\boldsymbol{\alpha}$, $\boldsymbol{\pi}$, and $\boldsymbol{\sigma}$ at a temperature of 10 K (upper) and 300 K (lower), respectively. All transitions are starting from the $^4I_{15/2}$ ground state level, the respective excited state levels are indicated.

distribution of the local field at the erbium sites, yielding the broadening found in the spectra.

2.4. Judd–Ofelt analysis

Electric dipole transitions between two states of $4f^N$ configuration of rare earth ions, which are forbidden for free ions, become allowed in the crystal field by mixing into the $4f^N$ configuration another configuration ($4f^{N-1}\,5d^1$) of opposite parity. The matrix elements of the electric dipole operator are calculated by considering the crystal field as a first-order perturbation.

According to the theory of Judd [32] and Ofelt [33], the line strengths for electric dipole transitions can be referred to three intensity parameters Ω_2, Ω_4, and Ω_6, the so-called Judd–Ofelt parameters. The line strength for a transition from an initial multiplet J to a final one J' is given by

$$S^{\text{ed, cal}}_{JJ'} = \sum_{t=2,4,6} \Omega_t |\langle 4f^n[\alpha SL]J||U^{(t)}||4f^n[\alpha' S'L']J'\rangle|^2. \quad (5)$$

In Eq. (5), the $|\langle\|U^{(t)}\|\rangle|^2$ are the squared reduced matrix elements of the unit tensor operators $U^{(t)}$ connecting the initial and final multiplets.

For magnetic dipole transitions, the line strength S^{md} is defined as

$$S^{\text{md}}[(S,L)J;(S',L')J'] = \frac{1}{4m^2c^2}|\langle (S,L)J||L+2S||(S',L')J'\rangle|^2 \quad (6)$$

with m – electron mass and c – velocity of light. Numerical values for the matrix elements in Eqs. (5) and (6) can be calculated according to Carnall et al. [34,35] and Weber [36]. The integral intensity B over an absorption band then can be written as

$$B = \int_{\text{band}} \alpha d\lambda = \frac{2\pi^2 e^2 \bar{\lambda}\rho}{3\varepsilon_0 ch(2J+1)n^2}\cdot\left(\frac{n(n^2+2)^2}{9}S^{\text{ed}} + n^3 S^{\text{md}}\right), \quad (7)$$

where α is the absorption coefficient, $\bar{\lambda}$ the mean absorption wavelength, e the electron charge, ρ the erbium concentration, ε_0 the vacuum permittivity, h Planck's constant, $(2J+1)$ the multiplicity of the ground level, and n the refractive index. In an optically anisotropic material like SBN, for the absorption coefficient and the refractive index the appropriate spatial averages have to be calculated, using the three fundamental polarization directions.

Eqs. (5)–(7) define a system of linear equations for the Ω_t which is over-determined – the number of absorption bands is larger than the number of Judd–Ofelt parameters. It can be solved applying a conventional least-square-fit solution scheme. Using the room-temperature absorption spectra, appropriate refractive indices [37], and the matrix elements calculated by Weber [36] and Carnall et al. [35], we calculated the Ω_t for different concentrations of Er^{3+}. The values derived did not show any dependence on the concentration which proves that – up to our highest concentrations – no interaction effects between different Er^{3+} ions affect the optical absorption. The Ω values are summarized in Table 1.

With the experimental and calculated absorption band intensities, B^{exp} and B^{calc}, the relative root mean square error (RRMSE) for the fit, defined as

$$\text{RRMSE} = \left(\frac{1}{n}\sum_{k=1}^{n}\frac{\left(B_k^{\text{exp}} - B_k^{\text{calc}}\right)^2}{\left(B_k^{\text{exp}}\right)^2}\right)^{1/2} \quad (8)$$

was found to be 18%. This can be regarded as a measure for the accuracy of the numerical results.

Table 1
Judd–Ofelt parameters Ω for Er^{3+} in strontium barium niobate.

Ω_2	Ω_4	Ω_6	
1.17	0.49	0.18	$\times 10^{-24}\,m^2$

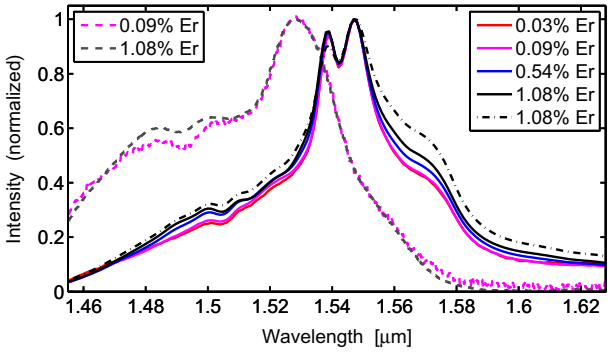

Fig. 3. 1.55 μm luminescence of erbium-doped SBN measured at room temperature on samples with different Er content (full lines). The dash-dotted line represents a spectrum measured at modified geometry (see text). For comparison, two of the corresponding absorption bands are plotted, too (dashed lines).

2.5. $^4I_{13/2} \Rightarrow {}^4I_{15/2}$ luminescence

The luminescence measurements on the main fluorescence band at 1.55 μm were performed on cube-shaped samples, typically 5∗5∗5 mm^3 sized, using an Amko 0.25 m monochromator and a suitable photodiode for detection. As excitation source a frequency-doubled Nd:YAG laser at 0.53 μm was used. Luminescence spectra for different erbium concentrations are shown in Fig. 3.

For comparison, two typical of the corresponding absorption spectra are shown, too – one for low, one for high erbium concentration. While the absorption bands do not show any expressed dependence on erbium concentration, the $^4I_{13/2} \Rightarrow {}^4I_{15/2}$ luminescence band broadens distinctly with increasing erbium content.

Possible explanations for this behavior include:

(1) A non-thermalized occupation of the 14 possible $^4I_{13/2}$ sublevels at low erbium content in contrast to a better thermalized one at higher concentration.
(2) Reabsorption of fluorescence light [38,39] could trap radiation and redistribute excitation energy from higher to lower energetic excited state. This would explain that the broadening mainly enhances the low-energy side of the luminescence band.

To decide between the two explanations, we modified the geometry exciting a sample deeper in the bulk. The enforced broadening (dash-dotted line in Fig. 3) indicates that the second explanation is to be favored and one has to deal with reabsorption effects.

2.6. Lifetime and quantum efficiency

To get information about the quantum efficiency of the $^4I_{13/2} \Rightarrow {}^4I_{15/2}$ transition we measured the luminescence decay following pulsed laser excitation. The results are plotted in Fig. 4. The strictly linear behavior in the semi-logarithmic representation proves a strongly exponential decay with a uniform decay time for each of the samples. The decay time, i.e., the lifetime of the initial level $^4I_{13/2}$, increases with increasing erbium content.

At low erbium concentrations the lifetime is approximately 3.4 ms, it increases up to approximately 5.7 ms for erbium concentrations around 1 mol%. The lifetimes for the various concentrations are plotted in the inset of Fig. 4.

As discussed before, SBN undergoes a structural phase transition from a ferroelectric to a paraelectric phase at temperatures between 310 and 360 K depending on the erbium concentration. To check the influence of this symmetry modification on lifetime and quantum efficiency, we measured all decay curves over the

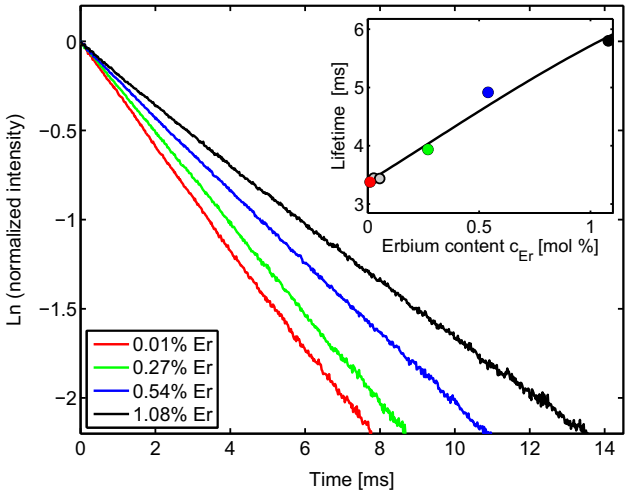

Fig. 4. Decay of the $^4I_{13/2} \Rightarrow {}^4I_{15/2}$ luminescence following pulsed excitation for SBN samples with different erbium content. In the inset the lifetimes derived from the decay curves are plotted; also shown is the fit using the reabsorption ansatz (see text).

temperature range 285–405 K. For all of our erbium concentrations the measured lifetimes were found to be constant throughout this temperature range. This indicates – in contrast to the behavior found, e.g., for europium [18] – that the luminescence properties of erbium are insensitive to the symmetry changes caused by the phase transition.

The spontaneous emission rate A, which determines the radiative lifetime of a transition, can be calculated as sum of electric and magnetic dipole contributions from the respective line strengths S^{ed} and S^{md} [40]

$$A_{J'J} = A^{ed}_{J'J} + A^{md}_{J'J} = \frac{16\pi^3 e^2}{3\epsilon_0 h(2J'+1)\bar{\lambda}^3}\left\{\frac{n(n^2+2)^2}{9}S^{ed}_{J'J} + n^3 S^{md}_{J'J}\right\}, \quad (9)$$

$\bar{\lambda}$ being the mean wavelength of the band, n the refractive index, and h, ϵ_0, e the usual constants.

Using the Judd–Ofelt parameters Ω_t and the transition matrix elements given by Weber [36] and Carnall et al. [35], we get the total spontaneous emission rate for the $^4I_{13/2} \Rightarrow {}^4I_{15/2}$ transition

$$A_{tot} = A_{ed} + A_{md} = 170\ s^{-1}. \quad (10)$$

The corresponding radiative lifetime of the $^4I_{13/2}$ level is 5.9 ms. Usually one would compare this value with the measured total lifetimes to calculate the radiative quantum efficiencies for the transition in different samples. The thus calculated efficiencies would reach approximately 95% at concentrations around 1 mol%.

Taking the previously discussed reabsorption into account, however, leads to different results. The time dependence of the upper level excess occupation N, i.e., the occupation difference to the thermal equilibrium state, can be described by the first order differential equation

$$\frac{dN}{dt} = -\frac{N}{\tau} = -\frac{N}{\tau_n} - \frac{N}{\tau_r} + \frac{N}{\tau_r}R, \quad (11)$$

where τ is the total lifetime, τ_n and τ_r are the nonradiative and the radiative lifetimes, respectively, and R is a factor describing the repopulation of the excited states by reabsorption of emitted light. Due to reabsorption, the total lifetime increases, radiation is trapped. Accordingly, the effective quantum efficiency decreases.

The factor R describing the reabsorption effects should be increasing with increasing erbium content c, albeit has to be kept less than one, therefore we use a one-parameter exponential ansatz

$$R = 1 - \exp(-ac) \quad (12)$$

with a constant fit parameter a. This ansatz defines R to depend linearly on the erbium concentration at low concentrations and to approach unity at very high concentrations. The strictly exponential decay even at our highest concentrations requires that R does not depend on N.

From a fit to our experimental decay time data – shown as the full line in the inset of Fig. 3 – the parameter a can be derived to be $a = 1.2\ (\text{mol\%})^{-1}$. The nonradiative lifetime τ_n is yielded from an extrapolation to zero erbium concentration, $\tau_n = 8.1$ ms. Comparing this value with the radiative lifetime results in a quantum efficiency of approximately 60% in the low concentration limit. Due to the reabsorption factor R in Eq. 11 the total lifetime is increased with increasing erbium concentration, radiation is trapped and thus delayed, less radiation escapes. Thus the effective quantum efficiency for our geometry decreases to approximately 30% at higher erbium concentrations. This contrasts highly to the efficiencies derived directly from the measured total and calculated radiative lifetimes without taking reabsorption effects into account.

2.7. Upconversion luminescence

The quantum yield in the 1.55 μm luminescence of erbium ions is known to be affected by upconversion. On the other hand upconversion may be utilized for the generation of light at shorter wavelengths. The typical luminescence bands found in upconversion spectra are shown in Fig. 5.

The spectra were measured using a Spex 0.75 m monochromator in combination with appropriate photomultipliers and a photon counting system. To show the band shapes, the intensities are normalized. As upconversion is a nonlinear process, the real intensities depend strongly on excitation intensity and on excitation wavelength.

Two processes usually control the upconversion in erbium, excited state absorption (ESA) and energy transfer upconversion (ETU). To distinguish, which of these is the dominating one for our erbium concentrations in SBN, we measured the decay times of all upconversion bands. For this purpose we used pulsed excitation at 0.8 μm and at 1.48 μm. For ETU one would expect decay times similar to the total lifetime of the $^4I_{13/2}$ level, for ESA shorter ones. For all bands the decay times measured were distinctly shorter than that expected for $^4I_{13/2}$ level ETU.

The measured decay times are listed in Table 2. For comparison, we calculated the radiative lifetimes for the transitions using the Judd–Ofelt parameters and the transition matrix elements as described above. From the comparison, the radiative fractions, i.e., the fraction of excited states decaying radiatively, are derived. These values are listed in Table 2, too.

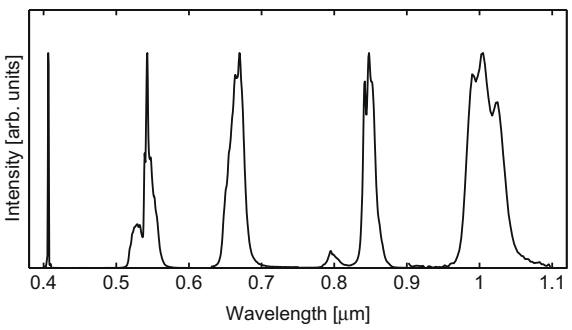

Fig. 5. Luminescence of erbium-doped SBN in the visible and near infrared spectral region due to upconversion. To show the different bands in a similar intensity scale, all intensities are normalized to the respective peak of the emission band.

Table 2
Measured total lifetimes, calculated radiative lifetimes, and there-from derived radiative fractions for the visible and near infrared upconversion bands in erbium-doped SBN (erbium content $\leqslant 0.6\%$).

Wavelength (μm)	Transition	Lifetime (ms)		Radiative fractions (%)
		Total	Radiative	
0.41	$^2H_{9/2} \Rightarrow {}^4I_{15/2}$	0.12	0.76	16
0.53, 0.55	$^2H_{11/2}$, $^4S_{3/2} \Rightarrow {}^4I_{15/2}$	0.11	1.2	9.2
0.67	$^4F_{9/2} \Rightarrow {}^4I_{15/2}$	0.08	0.88	9.1
0.85	$^4I_{9/2} \Rightarrow {}^4I_{15/2}$	0.10	17.6	1.3
1.00	$^4I_{11/2} \Rightarrow {}^4I_{15/2}$	0.82	12.5	6.6

All these experimental data show that ETU can be neglected – at least at our erbium concentrations up to 1 mol%. Accordingly all upconversion bands must be referred to ESA.

3. Summary

Besides defining the optical properties, erbium doping of strontium barium niobate crystals strongly affects the phase transition from the low-temperature ferroelectric to the high-temperature paraelectric phase of SBN. The transition temperature decreases linearly from 350 K for undoped SBN to approximately 315 K for a doping level of 1.1 mol% erbium. Due to the crystal structure of SBN doping with erbium does not seem to saturate, the distribution coefficient is found to remain constant. Thus the phase transition temperature might be shifted even further using higher doping concentrations, broadening the transition at the same time.

While the form of the absorption spectra is not affected by the erbium concentration, the form of the infrared luminescence band at 1.55 μm strongly depends on the erbium content and on the excitation geometry. This is due to reabsorption effects which thus have to be considered when the radiative quantum efficiency is derived from the radiative and the total lifetimes. Reabsorption can be included in the description of the decay time by an additional factor in the respective differential equation. Measuring the decay times for different concentrations and calculating a fit to these data yields the quantum efficiency as the extrapolation to the zero concentration limit. In the case of SBN, it is approximately 60%.

Decay time measurements on the upconversion bands show that only excited state absorption has to be considered, energy transfer upconversion may be neglected – at least up to 1 mol% erbium content.

Acknowledgement

Financial support from the Deutsche Forschungsgemeinschaft through the Graduate College *Nonlinearities of Optical Materials* is gratefully acknowledged.

References

[1] A.M. Glass, J. Appl. Phys. 40 (1969) 4699.
[2] R.R. Neurgaonkar, M.H. Kalisher, T.C. Lim, E.J. Staples, K.L. Keester, Mater. Res. Bull. 15 (1980) 1235.
[3] R.R. Neurgaonkar, W.K. Cory, J.R. Oliver, E.J. Sharp, M.J. Miller, G.L. Wood, W.W. Clark III, A.G. Mott, G.J. Salamo, B.D. Monson, SPIE 1148 (1989) 2.
[4] F. Kahmann, J. Höhne, R. Pankrath, R.A. Rupp, Phys. Rev. B 50 (1994) 2474.
[5] H.Y. Zhang, X.H. He, Y.H. Shih, L. Yan, J. Mod. Opt. 669 (1994) 6613.
[6] M. Wesner, C. Herden, R. Pankrath, D. Kip, P. Moretti, Phys. Rev. E 6403 (2001) 6613.
[7] A.S. Kewitsch, M. Segev, A. Yariv, G.J. Salamo, T.W. Towe, E.J. Sharp, R.R. Neurgaonkar, Appl. Phys. Lett. 64 (1994) 3068.
[8] A.R. Tunyagi, M. Ulex, K. Betzler, Phys. Rev. Lett. 90 (2003) 243901.
[9] R. Fischer, S.M. Saltiel, D.N. Neshev, W. Krolikowski, Y.S. Kivshar, Appl. Phys. Lett. 89 (2006) 191105.
[10] R. Fischer, D.N. Neshev, S.M. Saltiel, A.A. Sukhorukov, W. Krolikowski, Y.S. Kivshar, Appl. Phys. Lett. 91 (2007) 031104.
[11] M. Ulex, R. Pankrath, K. Betzler, J. Cryst. Growth 271 (2004) 128.
[12] L. Cross, Ferroelectrics 76 (3–4) (1987) 241.
[13] C. David, T. Granzow, A. Tunyagi, M. Wöhlecke, T. Woike, K. Betzler, M. Ulex, M. Imlau, R. Pankrath, Phys. Stat. Sol. (a) 201 (2004) R49.
[14] J.F. Scott, J. Phys.-Condens. Matter 18 (31) (2006) 7123, doi:10.1088/0953-8984/18/31/007.
[15] W. Kleemann, J. Phys.-Condens. Matter 18 (41) (2006) L523, doi:10.1088/0953-8984/18/41/L03.
[16] U. Voelker, U. Heine, C. Goedecker, K. Betzler, J. Appl. Phys. 102 (11) (2007) 114112, doi:10.1063/1.2821754.
[17] T. Granzow, T. Woike, W. Rammensee, M. Wöhlecke, M. Imlau, R. Pankrath, Phys. Stat. Sol. (a) 197 (2003) R2.
[18] Ä. Andresen, A.-N. Bahar, D. Conradi, I.-I. Oprea, R. Pankrath, U. Voelker, K. Betzler, M. Wöhlecke, U. Caldiño, E. Martín, D. Jaque, J. García Solé, Phys. Rev. B 77 (2008) 214102, doi:10.1103/PhysRevB.77.214102.
[19] M.O. Ramírez, D. Jaque, L.E. Bausá, J. García Solé, A.A. Kaminskii, Phys. Rev. Lett. 95 (26) (2005) 267401, doi:10.1103/PhysRevLett.95.267401.
[20] A. Rodenas, C. Jacinto, L.R. Freitas, D. Jaque, T. Catunda, Phys. Rev. B 79 (3) (2009) 033108, doi:10.1103/PhysRevB.79.033108.
[21] J.J. Romero, D. Jaque, J. García Solé, A.A. Kaminskii, Appl. Phys. Lett. 78 (2001) 1961.
[22] P. Molina, M.d.l.O. Ramirez, L.E. Bausa, Adv. Funct. Mater. 18 (5) (2008) 709, doi:10.1002/adfm.200700905.
[23] N.C. Giles, J.L. Wolford, G.J. Edwards, R. Uhrin, J. Appl. Phys. 77 (1995) 976.
[24] M.H. Li, X.W. Xu, T.C. Chong, H. Kumagai, M. Hirano, Ferroelectrics 230 (1999) 529.
[25] M.H. Li, T.C. Chong, X.W. Xu, H. Kumagai, J. Cryst. Growth 225 (2001) 479.
[26] H. Liu, G.K. Liu, S.T. Li, J.V. Beitz, F.E. Fernandez, J. Appl. Phys. 91 (2002) 129.
[27] M. Bettinelli, A. Speghini, A. Ródenas, P. Molina, M. de la, O. Ramírez, B. Capote, D. Jaque, L.E. Bausá, J. García Solé, J. Lumines. 122 (2007) 307.
[28] M. Daldosso, A. Speghini, P. Ghigna, M.delaO. Ramirez, D. Jaque, L.E. Bausá, J. García Solé, M. Bettinelli, J. Alloys Compd. 451 (2008) 12.
[29] U. Caldino, P. Molina, M.O. Ramirez, D. Jaque, L.E. Bausa, C. Zaldo, L. Ivleva, M. Bettinelli, J. García Solé, Ferroelectrics 363 (2008) 150, doi:10.1080/00150190802026002.
[30] M. Ramirez, D. Jaque, L. Ivleva, L. Bausa, J. Appl. Phys. 95 (11, Part 1) (2004) 6185, doi:10.1063/1.1713026.
[31] G.H. Dieke, Spectra and Energy Levels of Rare Earth Ions in Crystals, Interscience Publishers/John Wiley & Sons, New York, London, Sydney, Toronto, 1968.
[32] B.R. Judd, Phys. Rev. 127 (1962) 750.
[33] G.S. Ofelt, J. Chem. Phys. 37 (1962) 511.
[34] W.T. Carnall, P.R. Fields, B.G. Wybourne, J. Chem. Phys. 42 (1965) 3797.
[35] W.T. Carnall, P.R. Fields, K. Rajnak, J. Chem. Phys. 49 (1968) 4424.
[36] M.J. Weber, Phys. Rev. 157 (1967) 262.
[37] C. David, A. Tunyagi, K. Betzler, M. Wöhlecke, Phys. Stat. Sol. (b) 244 (2007) 2127, doi:10.1002/pssb.200642370.
[38] C. Li, C. Wyon, R. Moncorge, IEEE J. Quantum Electron. 28 (4) (1992) 1209.
[39] M. Mattarelli, M. Montagna, L. Zampedri, A. Chiasera, M. Ferrari, G. Righini, L. Fortes, M. Goncalves, L. Santos, R. Almeida, Europhys. Lett. 71 (3) (2005) 394, doi:10.1209/epl/i2005-10092-4.
[40] R.D. Peacock, The intensities of lanthanide f-f transitions, in: J.D. Dunitz, P. Hemmerich, R.H. Holm, J.A. Ibers, C.K. Jorgensen, J.B. Neilands, D. Reinen, R.J.P. Williams (Eds.), Structure and Bonding, vol. 22, Springer, Berlin, 1975, p. 83.